Key role of the Madden-Julian Oscillation on humid heatwaves

Claire Rocuet,[a,b] Takeshi Izumo,[b,c] Bastien Pagli,[a,b,c] Neil J. Holbrook,[d,e]

Sophie Cravatte, [c,f] Marania Hopuare, [a,g] Maxime Colin [h]

[a] *Université de la Polynésie Française (UPF), Tahiti, French Polynesia*

[b] *UMR241 SECOPOL laboratory (IRD/UPF/IFREMER/ILM), Tahiti, French Polynesia*

[c] *Institut de Recherche pour le Développement (IRD), France*

[d] *Institute for Marine and Antarctic Studies, University of Tasmania, Hobart, Tasmania, Australia*

[e] *Australian Research Council Centre of Excellence for the Weather of the 21st Century, University of Tasmania, Hobart, Tasmania, Australia*

[f] *Université de Toulouse, LEGOS (CNES/CNRS/IRD/UT3), Nouméa, Nouvelle-Calédonie*

[g] *GePaSud Laboratory, Tahiti, French Polynesia*

[h] *Leibniz Centre for Tropical Marine Research, ZMT, Bremen, Germany*

Corresponding author: Claire Rocuet, claire.rocuet@doctorant.upf.pf

Submitted to *Journal of Climate* on 19/08/2025 (under review)

ABSTRACT

Humid heat stress and heatwaves pose significant risks for living organisms, from humans and wildlife to insects, with wide-ranging health, ecological, and socio-economic impacts that are expected to worsen with climate change. How large-scale climate modes drive the week-to-month variability of humid heat remains poorly understood at the global scale, hindering accurate forecasts necessary for risk-management measures, notably in the heavily populated and ecologically fragile regions of the tropics and subtropics. With forecast lead times up to several weeks, the Madden-Julian Oscillation (MJO), a global-scale intraseasonal tropical atmospheric wave circumnavigating Earth in around 30-60 days, provides considerable predictability for weather conditions, and meteorological and oceanic extremes. Here we show that the MJO, and the associated boreal summer intraseasonal oscillation (BSISO), have a significant influence on humid heatwaves over much of the tropics and subtropics across all seasons, both over terrestrial and marine regions. Humid heatwave likelihood can double or halve, depending on the MJO phase, in large areas of the Earth. The MJO/BSISO's influence on wet-bulb temperature is primarily via specific humidity rather than dry-bulb temperature anomalies. We find that specific humidity anomalies are influenced by horizontal advection of moisture in the planetary boundary layer, particularly in the subtropics where advection of the climatological moisture gradient by MJO-related anomalous winds is the dominant term.

SIGNIFICANCE STATEMENT

The aim of this study is to better understand how large-scale, intraseasonal tropical climate modes shape the occurrence of humid heatwaves, prolonged periods of hot and humid conditions, that threaten human health, ecosystems, and economies, especially across the tropics and subtropics. We show that the Madden–Julian Oscillation (MJO) and the boreal summer intraseasonal oscillation (BSISO) strongly influence when and where these extremes occur at the global scale. Depending on its phase, the MJO can either greatly increase or reduce the likelihood of a humid heatwave, mainly through changes in humidity driven by large-scale wind patterns. Since both the MJO and BSISO are predictable weeks in advance, our findings highlight their potential to improve early warnings of humid heat extremes.

1. Introduction

Global air temperature has risen since the pre-industrial period (IPCC, 2023) with the past ten years (2015-2024) all being in the top ten of the warmest years in global temperature data records going back to 1850 (NOAA, 2025). Global warming trends and associated increased extreme events such as heatwaves have, for a long time, focused on measurements of 'dry-bulb' temperature (Horton et al., 2015; Ji et al., 2014; Perkins et al., 2012; Perkins-Kirkpatrick & Lewis, 2020; Seneviratne et al., 2014). However, humid heat, the combination of high temperatures and humidity, has gained significant attention in the last decade (Sherwood & Huber, 2010; Buzan & Huber, 2020; Raymond et al., 2021; Rogers et al., 2021; Russo et al., 2017; Sherwood, 2018). Extremes in humid heat are considered harder to bear than hot and dry conditions. Importantly, high humidity inhibits the cooling effect of the evaporation of sweat on the skin's surface. When combined with high air temperature, it poses a health risk to humans (Hanna & Tait, 2015) and to other mammals that thermoregulate similarly to humans with usually similar body temperatures ($\pm$1-2°C) (Hafez, 1964). Moreover, humid heat does not need to be extreme to have consequences on the quality of life of humans in their day-to-day activities, such as work, education, sporting activities and hobbies (Vanos et al., 2023). The impacts of humid heat are felt in many regions around the globe on public health, energy demand and economic productivity for billions of people (Dunne et al., 2013; Mora et al., 2017; Chen et al., 2020; Raymond et al., 2020; Buzan & Huber, 2020).

Heat stress is recognised as one of the leading cause of weather-related death (Buzan et al., 2015; Ebi et al., 2021). This is why over 120 thermal stress indices have been developed over the years in an attempt to predict heat stress and its physiological responses (Buzan & Huber, 2020). Most of these metrics use atmospheric variables such as surface air temperature, humidity, pressure, winds and solar radiation. Some evaluate heat stress in terms of accumulated stress over several days or the rate of change in temperature while others are issued from complex prognostic physiology models that assess thermal stress (Buzan et al., 2015; Di Napoli et al., 2019; Vanos et al., 2023).

However, various studies still point to the combination of air temperature and humidity, in particular the wet-bulb temperature (Tw), as the best indicator for the environmental

conditions conducive to heat stress on human health (Sherwood & Huber, 2010; Hanna & Tait, 2015; Li et al., 2018; Raymond et al., 2020, 2021; Vanos et al., 2023). Tw refers to the temperature a parcel of air reaches when it is cooled to saturation by the process of evaporation and is widely used in climatology and meteorological studies assessing humid heat (Raymond et al., 2017; Buzan & Huber, 2020; Raymond et al., 2021; Ivanovich et al., 2022; Speizer et al., 2022; Y. Zhang et al., 2024). When the air is saturated (100% relative humidity), Tw equals the dry-bulb air temperature. Importantly, Tw is a useful metric for evaluating the effectiveness of evaporative cooling via sweating: once it exceeds skin temperature (~35°C), the body can no longer dissipate heat efficiently, regardless of adaptations such as clothing, activity level, or acclimation (Sherwood & Huber, 2010). As such, Tw represents a fundamental thermodynamic limit to human heat tolerance and is therefore used here to measure humid heat stress.

Projections of the spatial distribution of future surface air temperature trends show that the fastest warming is expected in the high-latitude regions of the northern hemisphere, with up to +1°C per decade projected for the near-term (2025–2049) period of the 21st century under the high emissions scenario representative concentration pathway 8.5 (RCP8.5) (Fan et al., 2020) – that is, a pathway leading to 8.5 Wm^{-2} of additional radiative forcing by the end of the 21st century. However, the tropics, which include some of the most densely populated regions with unique biodiversity, are set to experience a stronger increase in specific humidity than higher latitudes, because of the non-linearity of the Clausius-Clapeyron relation (Song et al., 2022). Compared to other regions, the tropics are already subject to particularly intense hot and humid conditions (Matthews et al., 2017; Rogers et al., 2021; Song et al., 2022). It is the exposure of humans and other animals to these conditions, particularly when outdoors, unprotected, or lacking adequate insulation, that poses a significant health hazard. These regions are expected to become permanently stressful all year round for humans (and more generally for animals) with extremes in humid heat predicted to increase in frequency and intensity even under relatively small increases in the global average temperature (Buzan et al., 2015; Coffel et al., 2017; Mora et al., 2017; Li et al., 2018; Rogers et al., 2021; Song et al., 2022). Superimposed on this long-term warming trend, temperature extremes, particularly heatwaves, will contribute to additional stress and exacerbate health risks for exposed populations. There is therefore an urgent need to better understand the drivers of humid heat variability and extremes.

El Niño–Southern Oscillation (ENSO) has been identified as the dominant large-scale driver for global humid heat anomalies in the tropics and subtropics (Raymond et al., 2020; Speizer et al., 2022), with implications for reliable forecast of extreme humid heat events months in advance (Y. Zhang et al., 2024). Another large-scale climate mode, the Madden-Julian oscillation (MJO), and the associated boreal summer intraseasonal oscillation (BSISO), has been suggested to modulate humid heat and humid heatwaves in two specific regions over boreal summer, the Persian Gulf and South Asia (Ivanovich et al., 2022). However, to our knowledge, its influence on the intraseasonal variability of humid heatwaves at the global scale has not yet been studied (the intraseasonal timescale being defined as signals with periods of about 20 to 100 days). The MJO is the primary mode of large-scale intraseasonal variability in the tropical atmosphere (C. Zhang, 2005, 2013). It is characterised by alternating periods of increased cloud cover, precipitation, and low-level wind convergence, that are associated with enhanced convection (active phase, lasting one to two weeks locally), and periods of clear skies, reduced precipitation, and drier and more stable air (inactive phase). These alternations (30-60 days period) result from the eastward propagation of a convective envelope at a speed of about 5 m/s over the Indo-Pacific warm pool (i.e. the tropical eastern Indian Ocean and western Pacific - roughly the eastern hemisphere - with sea surface temperature (SST) above about 28°C (in present climate)) where atmospheric deep convection and related precipitation are climatologically large. East of 180° into the western hemisphere, it propagates faster, around 10 to 15 m/s, accompanied by a rapid weakening of the convective signal as moist equatorial Kelvin waves circumnavigating the Earth along the equator take over. The BSISO, that can be seen as a seasonal variation of the same underlying dynamics as the MJO (S. Wang & Sobel, 2022), is essentially present in the Northern Hemisphere in boreal summer, has a southeast-northwest-tilted structure in precipitation anomalies from South Asia to the western Pacific Ocean and propagates north-eastward with a period of about 30-45 days (S. Wang et al., 2018; S. Wang & Sobel, 2022). We can classify the various phases of the MJO and track its progression through eight different areas/phases along the equator thanks to indices such as the Realtime Multivariate MJO (RMM) index (Wheeler & Hendon, 2004), or the all-season outgoing longwave radiation (OLR)-based MJO index (OMI) (Kiladis et al., 2014). Here we mainly use the OMI, argued to capture better the signal of both the MJO and BSISO and to reproduce the signal's northward propagation during the boreal summer (L. Wang et al., 2018; Ivanovich et al., 2022).

The MJO/BSISO influences weather conditions in the tropics, such as precipitation, winds, air temperature, swell (C. Zhang, 2013) and extreme events such as tropical cyclones and marine heatwaves (Camargo et al., 2009; Gregory et al., 2024; Dutheil et al., 2024), and has motivated numerous studies in recent years aiming to improve the representation of these modes in subseasonal-to-seasonal forecast models, due to the potential benefits to society (White et al., 2017, 2022). Today, dynamical forecasts exhibit significant skill prediction of about 2 to 4.5 weeks in advance (Jiang et al., 2020; Kim et al., 2018). These skills are expected to improve in the future with advances in artificial intelligence (AI) techniques (Delaunay & Christensen, 2022; Martin et al., 2022). The MJO/BSISO thus provide a significant forecasting potential in the tropics, offering a window of time to anticipate associated extreme events and activate responses early to mitigate or lessen their impacts.

Here we aim to understand and quantify the influence of the MJO and BSISO on humid heat stress throughout the tropics and subtropics, using Tw as our metric. We examine the likelihood of extreme humid heat events, humid heatwaves (HHWs) across different MJO/BSISO phases and seasons. Given the strong role of specific humidity in driving Tw anomalies, we also analyse how the MJO modulates specific humidity through horizontal advection. Finally, we discuss the broader implications of our findings, including the potential for predicting humid heatwaves weeks in advance.

2. Data and methods

a. Data

Humid heat, heat stress metrics, and synoptic conditions are analysed using hourly data at the surface level averaged into daily time-steps from the European Centre for Medium-Range Weather Forecasts (ECMWF) Reanalysis Version 5 (ERA5) between 1979 and 2020 (Hersbach et al., 2020). This includes the 2m air temperature, the 2m dewpoint temperature, the surface pressure, specific humidity at 950hPa, and the 10m and 950hPa zonal and meridional wind components on a global 0.25°x 0.25° longitude-latitude grid. The ERA5 data set does not directly provide the 2-m specific humidity. Therefore, we calculate it using the daily averaged 2-m dewpoint temperature (T_D) in Kelvin and surface pressure (p) in Pa,

considering the molecular mass ratio of water vapor and air (ε) of 0.621981. The specific humidity (q) in kg/kg is determined as follows:

$$q = \frac{\varepsilon e(T_D)}{p - (1-\varepsilon)e(T_D)}$$

(1)

where e, expressed in Pa, represents the water vapor pressure calculated using the August–Roche Magnus formulation of the Clausius–Clapeyron equation (see Equation 2 in SI)

The total precipitation rate, a useful indicator for deep convection in the tropics and associated with propagation of the MJO, is examined using the Global Precipitation Climatology Project (GPCP) Version 1.3 One-Degree Daily Precipitation Data Set (Huffman et al., 2001). This dataset provides daily merged analysis of precipitation combining satellite observations and surface rain gauge data on a global 1.0° by 1.0° longitude-latitude grid from 1996 to 2020. Note that this period available for GPCP is shorter than for the other variables, but is not an issue as this 25-year period is already sufficiently long to estimate MJO-related precipitation anomalies; precipitation not being the focus of the present study, we use it mainly to indicate where the MJO active phase is, as a landmark for readers most familiar with MJO convective anomalies.

b. Calculation of wet-bulb temperature

Wet-bulb temperature (Tw) (Sherwood, 2018) is typically schematised as being measured by wrapping a water-soaked wick around a thermometer bulb in a well-ventilated area, allowing evaporation to cool it (present sensors are now essentially electronic devices). Following Ivanovich et al. (2022), we calculate the wet-bulb temperature from the daily averaged surface temperature, pressure, and dewpoint temperature using the Davies-Jones method (Davies-Jones, 2008; Buzan et al., 2015). Davies-Jones (2008) outline various methods to calculate Tw. We have followed the most accurate equations used in Buzan et al. (2015) (see their Appendix A for more details). For comparison with other heat stress indices, simplified wet-bulb globe temperature (sWBGT) and Heat Index (HI), see the Supplementary Information.

c. MJO Index

Several indices are available for characterizing the propagation and amplitude of the MJO, derived from empirical orthogonal function (EOF) analysis of the spatial and temporal patterns of tropical convection and/or circulation. These metrics use observations to compute the principal components (PCs) serving as indices for diagnosing various MJO characteristics (S. Wang et al., 2018). The Realtime Multivariate MJO (RMM) index (Wheeler & Hendon, 2004) is based on satellite remote-sense outgoing longwave radiation (OLR) satellite data, and 850 hPa and 200 hPa zonal winds. Meanwhile, the all-season OLR-based MJO Index (OMI) (Kiladis et al., 2014) is another index argued to better capture the signal of both the BSISO and MJO, and reproducing the signal's north-eastward propagation during the boreal summer (S. Wang et al., 2018; Ivanovich et al., 2022). Figure 1 and Suppl. Fig. 1, based on OMI and RMM respectively, indeed confirm that the OMI is more all-round for our study aiming at quantifying the influence of MJO on humid heat for all the seasons separately. Thus, we use the OMI as our default MJO/BSISO index and use the well-known RMM index for comparison. The OMI index dataset used here is provided by the NOAA PSL, Boulder, Colorado, USA, via their website: https://psl.noaa.gov/mjo/mjoindex/. Meanwhile, The RMM index dataset is provided by the BOM and is available online: http://www.bom.gov.au/climate/mjo/graphics/rmm.74toRealtime.txt. The OMI involves an EOF analysis of 30–96-day eastward only filtered daily OLR data between 20°N and 20°S using a 121-day sliding window centred on each day of the year to capture the seasonal shifts of the MJO from 1979-2012. The 20-96 day filtered daily OLR data from 1979 to 2021, including both eastward and westward wavenumbers (up to zonal wavenumber 72), are then projected onto the corresponding spatial EOFs associated with that day of the year using PC analysis, reducing the data to the first two principal components (PC1 and PC2), which effectively represent the MJO and BSISO's variability. This approach ensures the OMI's adaptability to seasonal changes and provides a robust measure of the MJO's phase and strength. To align the OMI with the RMM convention for comparison, the sign of the OMI PC1 is reversed, and the principal component ordering is swapped, making OMI(PC2) equivalent to RMM1 and -OMI(PC1) equivalent to RMM2. The combination of PC1 and PC2 produces a two-dimensional phase space divided into 8 sections, representing the 8 phases of the MJO. It is used to measure the location and amplitude of the active convective pattern of the MJO. We consider the MJO to be active when the amplitude, i.e. the module of (OMI1, OMI2), is >1. Hence, only days when this criterion is met are considered (sensitivity

tests using different criteria, e.g. 2/3 gave similar results, with slight changes in anomaly amplitudes as expected). Note that the number of days per phase is not uniform across all phases, particularly during the boreal summer (see Supplementary Table 1), Tw composite analyses were also produced using the RMM index (not shown), with qualitatively similar results (but with some expected differences consistent with the differences seen in precipitation anomalies between Figure 1 using OMI and Suppl. Fig. 1 using RMM).

d. Band-pass filter and composite analysis

ERA5 hourly data were initially interpolated to a 1° by 1° longitude-latitude grid and aggregated into daily averages (i.e. same spatiotemporal resolution as GPCP). The daily climatology (e.g. Suppl. Fig. 2 and 3) and anomalies were computed for the entire available time periods of the ERA5 and GPCP datasets. A 20–96-day passband filter was applied to the daily anomalies using the difference of two lowpass Lanczos filters (window length of 192 days, half-power frequencies of 1/20 day^{-1} for the high frequency filter and 1/96 day^{-1} for the lower frequency filter). Composites were generated by averaging the anomaly field data over all the days falling within each MJO phase, and with MJO amplitude>1, using the OMI index for a particular season. To evaluate if the composites of the field anomalies significantly differ from zero at the 95% confidence level, statistical significance was assessed using a two-tailed student *t*-test. The number of effective degrees of freedom associated with each phase was calculated based on the discontinuous time-series, assuming an effective degree of freedom every 5 days (an approximation based on Equation 30 of Bretherton et al. (1999). The number of days for each phase for each season for the 1979-2020 period is presented in Supplementary Table 1. Tw anomalies are normalised after dividing them by the standard deviation of the unfiltered Tw daily anomalies (i.e. the amplitude of the whole intraseasonal and interannual variability, Suppl. Fig. 4) for each phase within the given season. The high percentages found highlight the key contribution of the MJO to humid heat variability.

e. Extreme Tw and humid heatwaves threshold

Although various definitions and methods have been previously applied to detect heatwaves (Peterson et al., 2001; Perkins & Alexander, 2013; Zuo et al., 2015; Barriopedro et al., 2023), generally, a heatwave is defined as an extreme weather event characterized by unusually high temperatures, exceeding what is normally expected for a specific location and time of the year, for an extended period. Here, adapting the method from Perkins and Alexander (2013) we identified HHWs when the daily 90th percentile of Tw was exceeded for

at least 3 consecutive days. This percentile represents the hottest 10% in daily mean values for that time of the year. It is based on a 15-day moving window of daily mean temperatures over 1979−2020 (e.g. for the 10th of July, we use all daily values from July 3nd to 17th for the 42 years to estimate the distribution and its 90th percentile). The percentage of the number of HHW days at each grid point for a given season ('Percentage_{season_mean}') is then calculated by counting the number of heatwave days for each season and dividing it by the total number of days in the same season. The same process is used to calculate the percentage of the number of extreme HHW days at each grid point for each MJO phase pair for a given season ('Percentage_{season_MJOphase}'). The ratio between (Percentage_{season_MJOphase}) and (Percentage_{season_mean}) is the ratio of change of HHW day likelihood due to the MJO. The occurrence anomaly is the difference between (Percentage_{season_MJOphase}) and (Percentage_{season_mean}). Brunner and Voigt (2024) identified a bias in heatwave identification when using longer running seasonal windows, however this bias is negligible in most of the tropics and the 15-days moving window here does not affect the result concerning the occurrence anomaly and likelihood of HHWs.

f. Contribution of specific humidity and dry-bulb temperature to Tw

The 2-m specific humidity q calculated in our study is a function of daily averaged 2-m dewpoint temperature (T_D) and surface pressure (p): $q(T_D, p)$ (see Equation 1 above). Assuming that variations in surface pressure are minimal (Lutsko, 2021) (confirmed by additional tests, not shown here) specific humidity can be expressed as:

$$q(T_D, p) \approx q(T_D, \overline{p}) \qquad (2)$$

where q is calculated using the time-varying T_D and the mean climatological $\overline{p}$.

Similarly, the T_w calculated using the Davies-Jones method (Davies-Jones, 2008; Buzan et al., 2015) is a function of daily averaged 2-m dry-bulb temperature (T_A), dewpoint temperature (T_D) and surface pressure (p); $T_w(T_A, T_D, p)$. Assuming the changes in surface pressure are small, we obtain $T_{w_{TD}}(\overline{T_A}, T_D, \overline{p})$ which is the wet-bulb temperature calculated with varying dewpoint temperature T_D and climatological mean $\overline{T_A}$ and $\overline{p}$ whilst $T_{wTa}(T_A, \overline{T_D}, \overline{p})$ is the wet-bulb temperature calculated with varying dry-bulb temperature T_A and climatological mean $\overline{T_D}$ and $\overline{p}$. The ratio between the anomalies of $T_{w_{TD}}$ and the anomalies of T_w $\left(\frac{T_{w_{TD}}'}{T_w'}\right)$ indicates the respective contribution of T_D (and thus, specific

humidity q) to the changes in Tw. The ratio between the anomalies of $T_{w_{TA}}$ and the anomalies of T_w $\left(\frac{T_{w_{TA}}'}{T_w'}\right)$ indicates the respective contribution of T_A to the changes in Tw.

g. Horizontal moisture advection and evaporation

The moisture budget equation to understand the rate of change of specific humidity anomalies is given as:

$$\frac{\partial q'}{\partial t} = \left(-\vec{V}.\nabla q\right)' - \left(\omega \frac{\partial q}{\partial p}\right)' - P' + E' \tag{5}$$

where $\frac{\partial q'}{\partial t}$ is the local time tendency of specific humidity anomalies. The terms on the right include the anomalous horizontal moisture advection $\left(-\vec{V}.\nabla q\right)'$, (V being the horizontal wind ∇q the horizontal humidity gradient), anomalous vertical advection $\left(\omega \frac{\partial q}{\partial p}\right)'$ (with ω the vertical pressure velocity) precipitation anomaly P' and evaporation anomaly E'.

Here, we focus on one term from the budget equation, specifically the intra-seasonally filtered anomalies of horizontal advection of specific humidity $\left(-\vec{V}.\nabla q\right)'$ at 950hPa (approximately 500m) as it corresponds to the average middle level of the boundary layer in the tropics. The zonal and meridional winds and specific humidity at the 950hPa pressure level are used here as an approximation for:

$$\left(-\overrightarrow{V_{950}}.\nabla q_{950}\right)' = -\left(u_{950}\frac{\partial q_{950}}{\partial x} + v_{950}\frac{\partial q_{950}}{\partial y}\right)' \tag{6}$$

The horizontal advection term is further partitioned into three components for a better attribution of the horizontal advection anomalies:

$$\left(-\overrightarrow{V_{950}}.\nabla q_{950}\right)' = \left(-\overrightarrow{V_{950}}'.\nabla \overline{q_{950}}\right) + \left(-\overline{\overrightarrow{V_{950}}}.\nabla q_{950}'\right) + \left(-\overrightarrow{V_{950}}'.\nabla q_{950}'\right) \tag{7}$$

3. Results

a. Key characteristics of the MJO

Figure 1 shows composite maps of the precipitation anomalies in the tropics and subtropics, with surface wind overlaid, for different MJO phase pairs for the two 'extended seasons', November to April (NDJFMA) and May to October (MJJASO), thus characterising the MJO cycle.
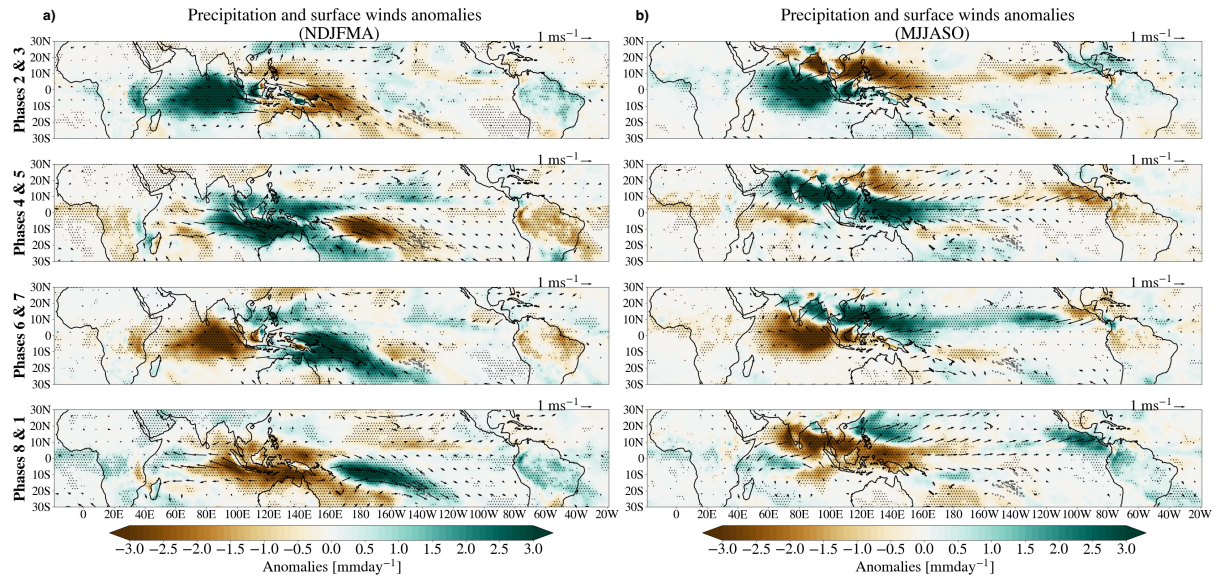

Fig. 1. Composite maps of intraseasonal anomalies of precipitation rate (colour shading) during the MJO phase pairs for a) the 'extended boreal winter' (from November to April, NDJFMA) b) the 'extended boreal summer' (from May to October, MJJASO). Stippling represents statistically significant precipitation anomalies at the 95% confidence level. 95% statistically significant surface (at 10m) wind anomaly vectors are overlaid (vectors are considered significant when either the zonal or meridional winds are significant). OMI (with amplitude of at least 1) is used for all MJO composites in the main text and supplementary material.

Surface wind and precipitation anomalies show the typical MJO characteristics and eastward propagation, which differ in winter and summer (Figure 1). In the extended boreal winter (austral summer, NDJFMA), during MJO phases 2&3, the MJO active phase has its strongest signals in the Indian Ocean just south of the equator. This is where the surface winds converge, favouring moisture convergence and deep convection. During MJO phases

12

4&5, MJO is usually at its peak over the Maritime Continent. During MJO phases 6&7, the MJO is active over the western Pacific. During MJO phases 8&1, the MJO is active along the South Pacific Convergence Zone (SPCZ) through to French Polynesia, while negative precipitation anomalies are centered over the Maritime Continent. In NDJFMA, the MJO-associated precipitation anomalies are located to the south of the equator following the seasonal southward migration of the Inter-Tropical Convergence Zone (ITCZ) in the Indian Ocean and of the SPCZ in the Pacific. During the extended boreal summer (austral winter, MJJASO), the precipitation anomalies are shifted northward, showing the BSISO and its north-eastward propagation in the Indian/Asian monsoon region as well as the MJO eastward propagation in the Pacific along the ITCZ until the Eastern Pacific Warm Pool. Here we do not differentiate between MJO and BSISO, considering the humid heat patterns to be associated with phases that describe the evolution of both oscillations. The wind anomalies show the classic Matsuno-Gill response to these precipitation/diabatic heating anomalies (Matsuno, 1966; Gill, 1980), deformed by the seasonally varying mean state (Watanabe & Jin, 2003).

b. Large-scale influence of MJO on humid heat

To quantify the contribution of the MJO to the intraseasonal variability of humid heat in the tropics and subtropics, composite maps of normalised Tw intraseasonal anomalies for the phases of the MJO during boreal winter and summer were prepared (Figure 2, see Suppl. Fig. 5 for intraseasonally filtered anomalies of Tw in °C). Interestingly, humid heat anomalies related to the MJO are statistically significant (at the 95% level) over large areas of the tropics and subtropics, for all phase pairs and seasons, both over land and ocean. Overall, most of the tropics and subtropics have statistically significant anomalies for at least one MJO phase. Instead of being confined in the ITCZ/SPCZ regions above warm waters as MJO-convection patterns tend to be, these Tw anomalies appear to extend well beyond the regions typically affected by precipitation and convection, with much wider spatial patterns.
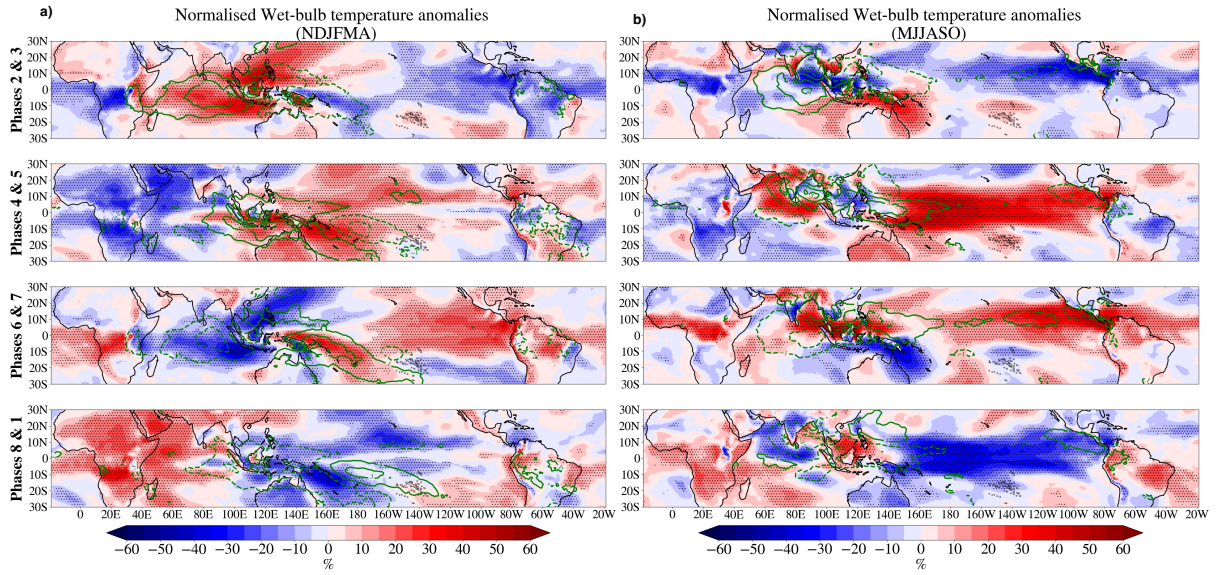
Fig. 2. Composite maps of intraseasonal anomalies of wet-bulb temperature (Tw, colour shading) given as a percentage of the total standard deviation (STD) of unfiltered Tw anomalies during the MJO phase pairs for a) the 'extended boreal winter' (from November to April, NDJFMA), and b) the 'extended boreal summer' (from May to October, MJJASO). Stippling represents statistically significant filtered Tw anomalies (at the 95% confidence level). Precipitation anomalies are overlaid as green contours (intervals of 1 mm day-1, with zero omitted).

The humid heat anomalies propagate eastward in both seasons all along the equatorial band, with a faster propagation speed reminiscent of moist equatorial Kelvin waves out of the convective regions (as shown in Figure 3), with the Tw, surface pressure anomalies and 10m zonal wind averaged in the equatorial waveguide (10°N-10°S, see Suppl. Fig. 6 and 7 for composites of surface winds and surface pressure). In addition, their spatial scales are similar to those of the atmospheric equatorial Kelvin and Rossby wave structures associated with the MJO (Seo & Kim, 2003). Amplitude-wise, the normalised anomalies of Tw (in % of the full Tw intraseasonal and interannual variability standard deviation (STD) shown in Suppl. Fig. 4) are generally large, up to ~40-50% in some regions (and still up to ~30-40% of the STD of Tw full variability including its seasonal cycle, not shown). Amplitude-wise in °C, the intraseasonally-filtered anomalies of Tw are often about +0.2-0.5°C, up to ~+1°C over some land masses such as Africa, the middle East, India, Asia/Southern China, and Australia (Suppl. Fig. 5 and Suppl. Fig. 2 for seasonal climatology) analysing each phase separately and 3-months period does not change the conclusions (not shown). Except over Australia and the equatorial Pacific Ocean, we generally observe higher amplitudes in °C during the boreal winter compared to the summer (Suppl. Fig. 5).

14

a) Wet-bulb temperature anomalies averaged over 10N-10S (NDJFMA)

b) Surface pressure averaged over 10N-10S (NDJFMA)

c) Wet-bulb temperature anomalies averaged over 10N-10S (MJJASO)

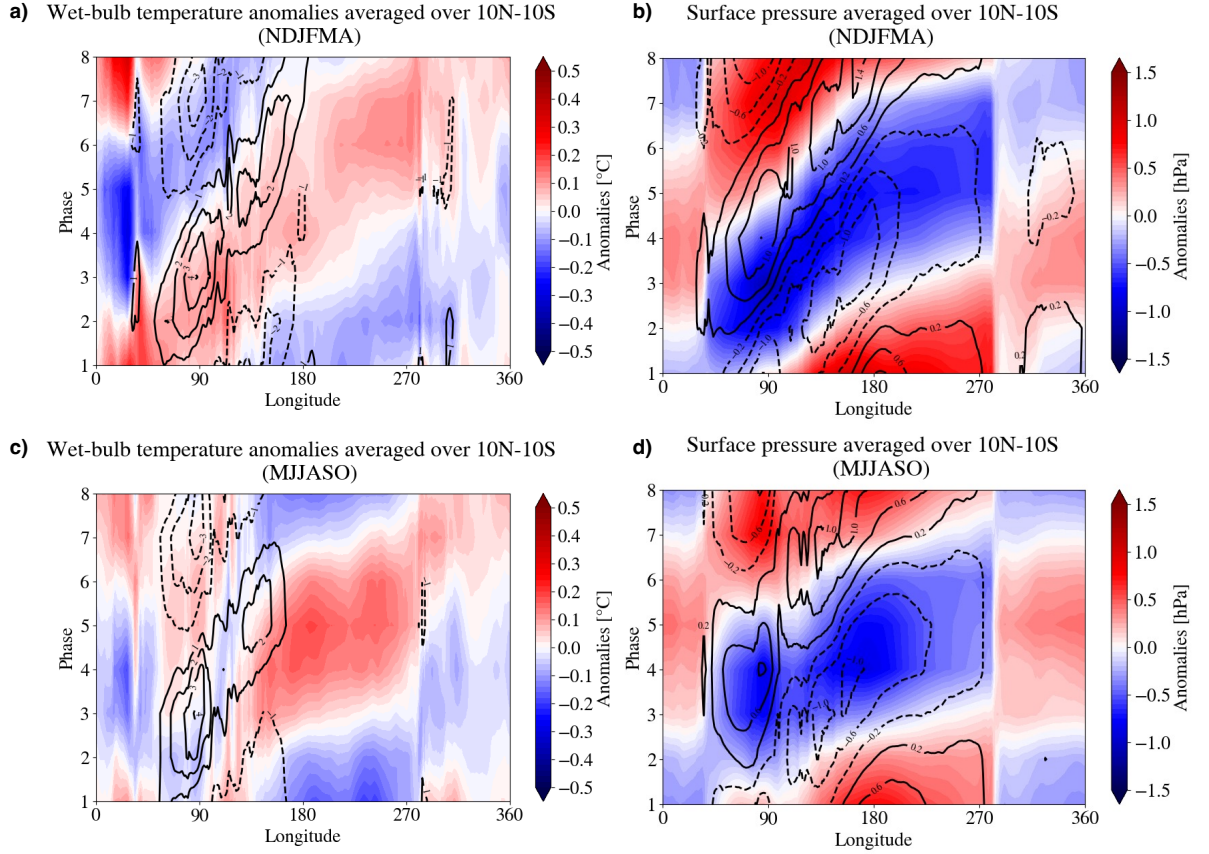**d)** Surface pressure averaged over 10N-10S (MJJASO)

Fig. 3. Hovmöller diagram of latitudinally averaged surface anomalies between 10°N and 10°S for composites of MJO phases 1-8 (y-axis) for a) wet-bulb temperature Tw with black contours showing precipitation anomalies (intervals of 1 mm day-1, with zero omitted), and b) surface pressure (hPa) with black contours showing zonal surface (10m) wind anomalies (intervals of 0.4 ms-1, with zero omitted). c)-d) same as a)-b) for MJJASO.

c. Regional influences of MJO on humid heat

At the regional scale, humid heat anomalies have more complex signatures, again with a strong seasonality. In regions with strong precipitation signals associated with the MJO during the extended boreal winter, such as the equatorial Indian Ocean (5S–5N, 50E–90E), the Maritime Continent (15S–15N, 90E–130E), Australia, and the southwest Pacific (30S–0, 150E–160W), positive (negative) Tw anomalies typically peak one to two phases before the peak of the positive (negative) precipitation anomalies. This indicates that in these areas, humid heat is often felt most intensely prior to the peak in convection, with conditions becoming cooler afterwards. In contrast, in regions with weaker convective signals, such as North Africa (10N–30N, 0–60E), South Tropical Africa (20S–5S, 10E–40E), the northwest Pacific (10N–30N, 120E–150E), and the northeast equatorial Pacific Ocean (0–10N, 120W–80W), the timing of the Tw anomalies is not necessarily linked to that of convection but tends

15

to be in phase, or have at most a lag of one phase, with both dry-bulb temperature and specific humidity anomalies (see Suppl. Fig. 8, 9 for composites of specific humidity and dry-bulb temperature anomalies respectively and Suppl. Fig 10 for phase distribution of each terms for the regions mentioned in NDJFMA). This suggests that the mechanisms driving changes in humid heat differ according to the presence or absence of strong convective signals.

During the extended boreal summer, the patterns are even more complex. Over oceanic regions where MJO-related convection is pronounced, regional differences emerge. For instance, in the North equatorial Indian Ocean (0–5N, 60E–95E), Tw and precipitation anomalies are almost out of phase, whereas in the western equatorial Pacific (5S–5N, 160E–150W), both reach their maximum during phases 4–5. In contrast, in the northeast tropical Pacific (5N–15N, 110W–80W), positive Tw anomalies peak just before the onset of enhanced precipitation. Over continental regions with strong intraseasonal precipitation anomalies, similar contrasts are found. For instance, in India, warm Tw anomalies coincide with rainfall peaks, while over mainland southeast Asia (10N–20N, 98E–109E) they occur roughly two phases earlier. These variations reflect differences in the relative influence of dry-bulb temperature and specific humidity anomalies on humid heat depending on the regions (Suppl. Fig. 8, 9 and 11). As shown in Supplementary Figure 11, in the North equatorial Indian Ocean, Tw anomalies begin to rise when specific humidity anomalies reach their maximum during the peak of rainfall, with the dry-bulb temperature only increasing afterwards. In the western equatorial Pacific, Tw change with specific humidity, lagging by one phase the dry-bulb temperature anomalies, while in the northeast tropical Pacific, Tw is in phase with both dry-bulb temperature and specific humidity. Over India, Tw seems to be primarily humidity-driven, with lower dry-bulb temperatures partially offsetting the strong moisture anomalies, whereas in mainland southeast Asia it reflects a combination of dry-bulb temperature and specific humidity influences. Similarly to the NDJFMA season, in MJJASO, regions with minimal MJO-related precipitation anomalies but significant humid heat anomalies, such as north-equatorial Africa (0–10N, 10–40E), South Tropical Africa, Australia, and southeastern South America (20S–0, 60W–40W), are likely driven by processes acting directly on temperature and humidity rather than by precipitation-associated convection. These contrasting patterns highlight the diversity of processes driving humid heat anomalies across both seasons, between oceanic and continental regions, and under varying

degrees of MJO-related precipitation. Such processes will be examined in detail in Sections e and f.

d. Extreme humid heat and heatwaves

Here we examine extremes in daily mean Tw values and classify them as Humid Heatwaves (HHWs), when at least 3 consecutive days exceed the 90th percentile climatological threshold for each calendar day. Figure 4 shows the ratio between the likelihood of humid heatwave day occurrence for a specific MJO phase pair and the season's average likelihood (i.e. a ratio of 1 means that the heatwave likelihood is as usual). The likelihood ratio strongly varies depending on the MJO phases, often between 1/2 and 2, and even up to about 1/3 and 3 for some regions/seasons. This means that the MJO's influence on humid heatwaves is so large that the likelihood of heatwave occurrence halves in some MJO phases and doubles in other phases in large areas of the tropics and subtropics. In other words, the likelihood can be four times larger in some MJO phases compared to other phases. This MJO influence is seen both on land surfaces, not only around the Persian Gulf, Indian subcontinent, and south Asia (consistent with Ivanovich et al., (2022)), but also over the large land masses of Africa, Australia and the Americas, and over oceans, notably the Pacific, Indian and Atlantic Oceans and their fragile islands and terrestrial ecosystems.
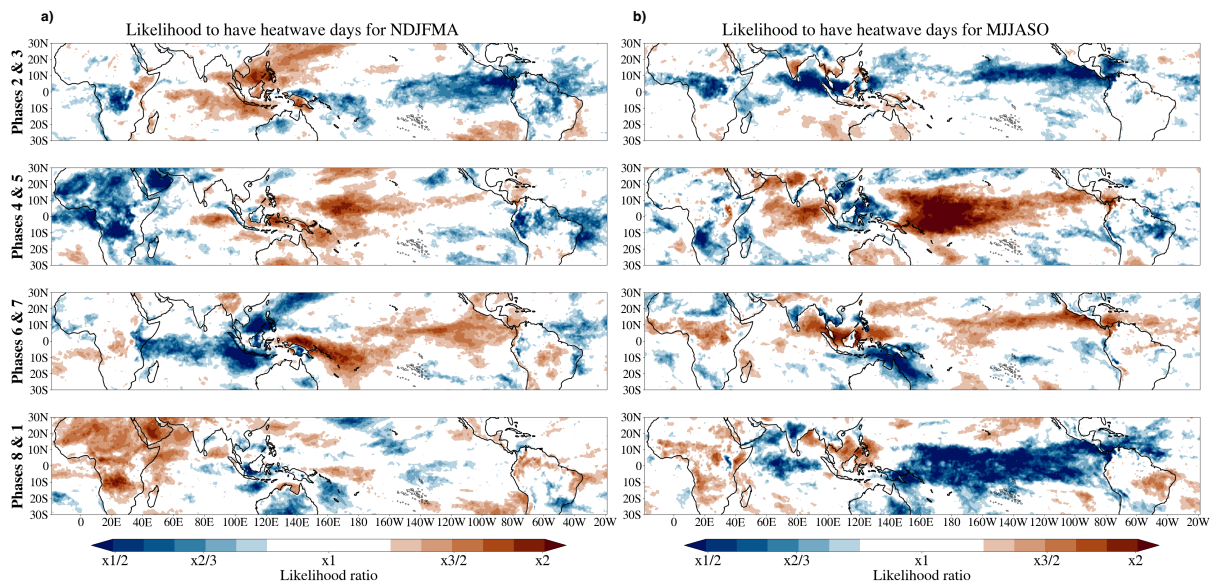

Fig. 4. Map of the ratio (i.e. the increase, if ratio >1, or decrease, if ratio <1, of humid heatwave days likelihood, colours shading in log scale) of the percentage of heatwave days (at least 3 consecutive days where Tw exceeds the daily 90th percentile values during each MJO phase pair, divided by the mean percentage, for a) the extended boreal winter (NDJFMA) and b) the extended boreal summer (MJJASO).

Here we describe the most notable HHW likelihood changes corresponding to MJO phase pairs. For the extended boreal winter (boreal summer), i.e. the austral summer (austral winter), HHWs occurring in the southern (northern) hemisphere and equatorial band will likely have larger impacts than those occurring in the northern (southern) tropics and subtropics because of the absolute heat stress that maximum absolute temperatures and humidity impose on humans and other mammals. In NDJFMA, during MJO phases 2&3, we observe a 1.5 to 2-fold increase (i.e. of about 50 to 100%) in the likelihood of extreme humid heat days in the western Indian Ocean, northwest Pacific and southeast Pacific. During MJO phases 4&5, HHW likelihood increases by about 50% in and around Australia, particularly in the southwest Pacific. It further increases to a doubled likelihood in phases 6&7 over the western Pacific islands and the SPCZ region. Finally, in MJO phases 8&1, extreme Tw days are more likely experienced over the African continent and Arabian Peninsula (up to about 2-fold increase), off the coast of northern Australia, and over part of the southeast Pacific.

In the extended boreal summer (MJJASO), during MJO phases 2&3, the HHW likelihood increases notably in south India, while it is reduced in the equatorial belt and in the tropical North Pacific. In phases 4&5, we have the largest likelihood ratio in the western Pacific, the likelihood being almost triple its usual value. A decrease is conversely seen in southern Africa, the Maritime Continent and South America. In terms of the percentage of heatwave days, it is in northern India (around Rajasthan desert and Madya Pradesh) and southern Bay of Bengal in MJO phases 4&5 that are the highest, reaching ~20% (Suppl Fig. 5 and 6). We observe that the highest likelihood of HHW occurrence is in regions where the amplitude of the Tw normalised anomalies is strongest (Figure 2). Therefore, these results demonstrate the ubiquitous influence of the MJO on Tw variability in the tropics and subtropics, favouring humid heatwaves or conversely cool dry spells depending on its phases.

e. Contributions of humidity and temperature to humid heat

In section c) we discussed that the variability of humid heat depends on whether it is more driven by high dry-bulb temperature, specific humidity or an even mix of both. Here we estimate more quantitatively the distinct contributions of specific humidity and dry-bulb temperature to humid heat. Figure 5 compares the percentage contribution of specific humidity and dry-bulb temperature to Tw intraseasonal anomalies. The specific humidity

18

dominates by far for most of the tropics for both seasons, (consistent with the results obtained by Buzan et al. (2015). Dry-bulb temperature plays a more dominant role than specific humidity only in climatologically dry arid lands such as North Africa, Pakistan and Nepal in NDJFMA, and northwest Africa and Chile in MJJASO. Over the tropical oceans, only specific humidity plays a dominant role regardless of the season. The dry-bulb temperature contribution can even be slightly negative in some specific regions such as the eastern tip of South America, the north of Australia and around Tanzania in NDJFMA, and the 10°N-20°N band in Africa, northern Kenya, India, Mexico and Guyana in MJJASO. This means that in these regions, the dry bulb temperature tends to compensate the specific humidity effect. E.g. negative dry-bulb temperature anomalies offset positive specific humidity anomalies. The 'negative' contribution of the dry-bulb temperature in these regions could be attributed to increased cloud coverage in those regions during humid MJO phases, but the lack of solar radiation decreases the dry-bulb temperature (i.e. through the cloud negative radiative feedback). Although specific humidity contributes most to Tw in most regions, sometimes dry-bulb temperature exhibits a stronger variability than humidity and can therefore exert a greater influence on humid heat than specific humidity such as in the Equatorial Indian Ocean and mainland Southeast Asia in MJJASO (Suppl. Fig. 11). To sum up, Tw anomalies over oceans and land are generally explained firstly by specific humidity, except in specific land areas such as deserts or when there is a strong variability of dry-bulb temperatures across the different MJO phases.
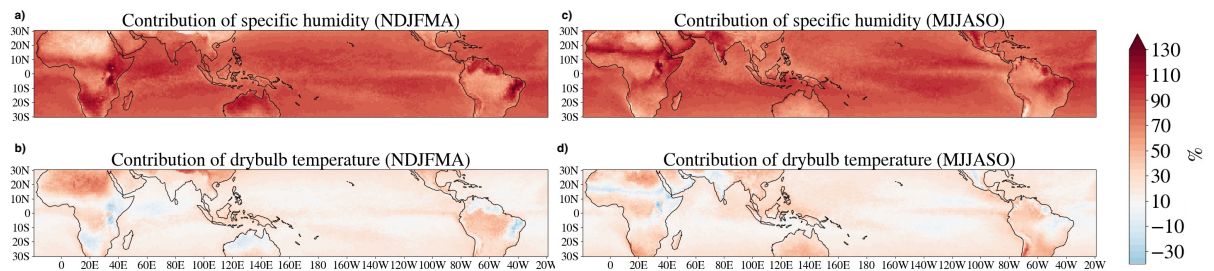

Fig. 5. Contribution map of specific humidity (via dewpoint temperature) and dry-bulb temperature to anomalies of Tw as percentage for a-b) NDJFMA and c-d) MJJASO.

f. MJO modulated moisture transport

Given the role of specific humidity in influencing Tw, it is important to understand how the large-scale anomalies of specific humidity are influenced by the MJO. Moisture (and related moist static energy) recharge of the lower troposphere to the east of the MJO active phase (and discharge under and west of it) is a well-known feature of the MJO's eastward

propagation (Seo & Kim, 2003; C. Zhang, 2005; C. Zhang et al., 2020) that has been extensively studied to understand MJO propagation mechanisms, but not to understand surface moisture variations related to the MJO, and related influence on humid heat. To do so, an in-depth moisture budget would be required but is beyond the scope of this study, and cannot be readily closed in atmospheric reanalysis (Kiranmayi & Maloney, 2011). Indeed, we expect to have several mechanisms at play behind the complex near-surface moisture budget. Since wind and windspeed have broad large-scale significant anomalies (Figure 3 b and d, Suppl. Fig. 6) and horizontal advection of specific humidity in the planetary boundary layer is an easily computed term of the moisture budget, we therefore analyse how it may explain the moistening and drying of some regions depending on MJO phases.

To understand surface moisture variations, we need to understand the specific humidity variations q' in the planetary boundary layer. As a rough approximation, we use 950hPa as our central level of the boundary layer. Indeed, the MJO-related anomalies of specific humidity q′ and of its tendency $\partial q'/\partial t$ at the surface are similar and strongly correlated to those at 950hPa (Suppl. Fig. 14 and 15). We thus examine the moisture horizontal advection anomalies at 950hPa, $-\left(\overrightarrow{V_{950}}.\nabla q_{950}\right)'$. The coefficients of the linear regression between $-\left(\overrightarrow{V_{950}}.\nabla q_{950}\right)'$ and $\partial q_{950}'/\partial t$ presented in Figure 6 are indicative of the role that horizontal advection in the planetary boundary layer plays in the intraseasonal variability of specific humidity for both seasons. In addition, to better understand the processes contributing to anomalous horizontal advection of specific humidity, we further decompose the horizontal advection term into three components: the anomalous wind acting on the climatological humidity field $\left(-\overrightarrow{V_{950}'}.\nabla \overline{q_{950}}\right)$, anomalous winds transporting anomalous specific humidity $\left(-\overrightarrow{V_{950}'}.\nabla q_{950}'\right)$, and climatological wind acting on anomalous specific humidity $\left(-\overrightarrow{\overline{V_{950}}}.\nabla q_{950}'\right)$ (Figure 7).

Linear regression between horizontal advection and dq'/dt at 950hPa in NDJFMA

Linear regression between horizontal advection and dq'/dt at 950hPa in MJJASO
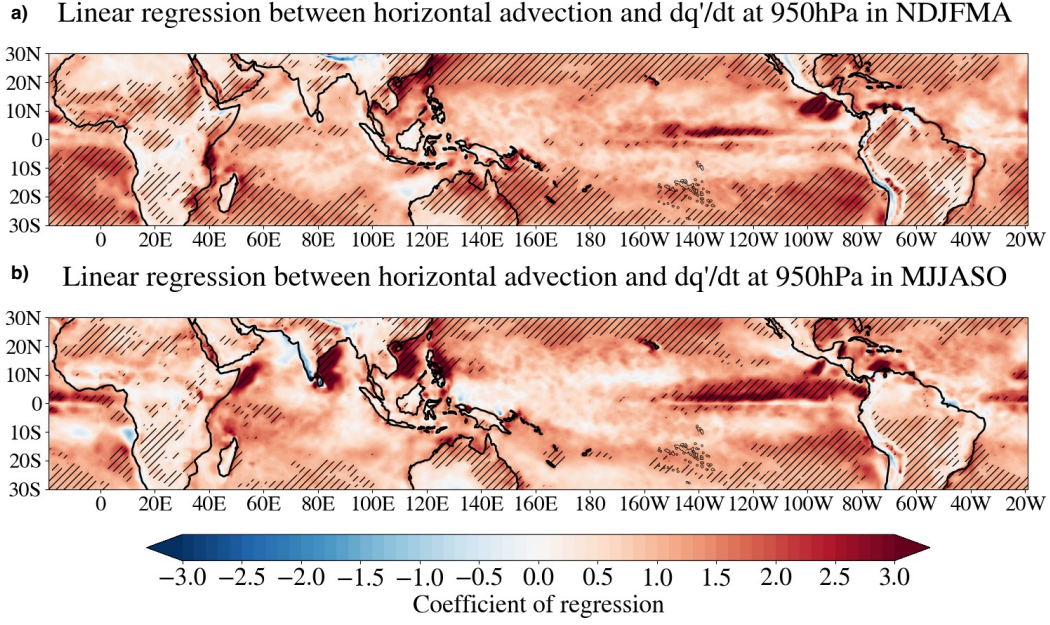
Fig. 6. Coefficient of regression (colour shading) and correlation (black hatching lines represents coefficient above 0.25) between horizontal advection anomalies at 950hPa and $\partial q'/\partial t$ at 950hPa for a) NDJFMA and b) MJJASO.

Overall, at the large scale, for both seasons, horizontal moisture advection in the planetary boundary layer influences specific humidity anomalies. Regions where the coefficient of regression values are higher than 1 are regions where reduced evaporation caused by reduced wind speeds (Suppl. Fig. 6.) may counteract the effect of advection. The role of advection is larger out of the equatorial band (except in the eastern equatorial Pacific and Atlantic in MJJASO). The strongest correlations are in the subtropics, where horizontal advection seems to play the dominant role in specific humidity intraseasonal variability, likely because of larger horizontal gradients of climatological moisture than near the equator (Suppl. Fig. 3), which relates to the sharp margins of the moist tropics (Mapes et al., 2018). The most obvious example to illustrate the mechanism at play is the Northwest subtropical Pacific in NDJFMA, where the moisture clearly increases when the southerly anomalies bring air from the climatologically more humid tropics (anomalous wind acting on the climatological humidity field $\left(-\overrightarrow{V_{950}}'.\nabla\overline{q_{950}}\right)$, and vice versa with northerlies (Suppl. Fig. 3 and 6)).

Only in a few specific regions are regression coefficients weakly negative, such as in the southeast Atlantic and southeast Indian Oceans, northeast Pacific, Arabian Sea in NDJFMA,

and north of the Maritime continent in MJJASO. There, the advection has a damping role (mainly the climatological wind advection of anomalous moisture $\left(-\overrightarrow{V_{950}}.\nabla q_{950}'\right)$, Figure 6 and Figure 7).
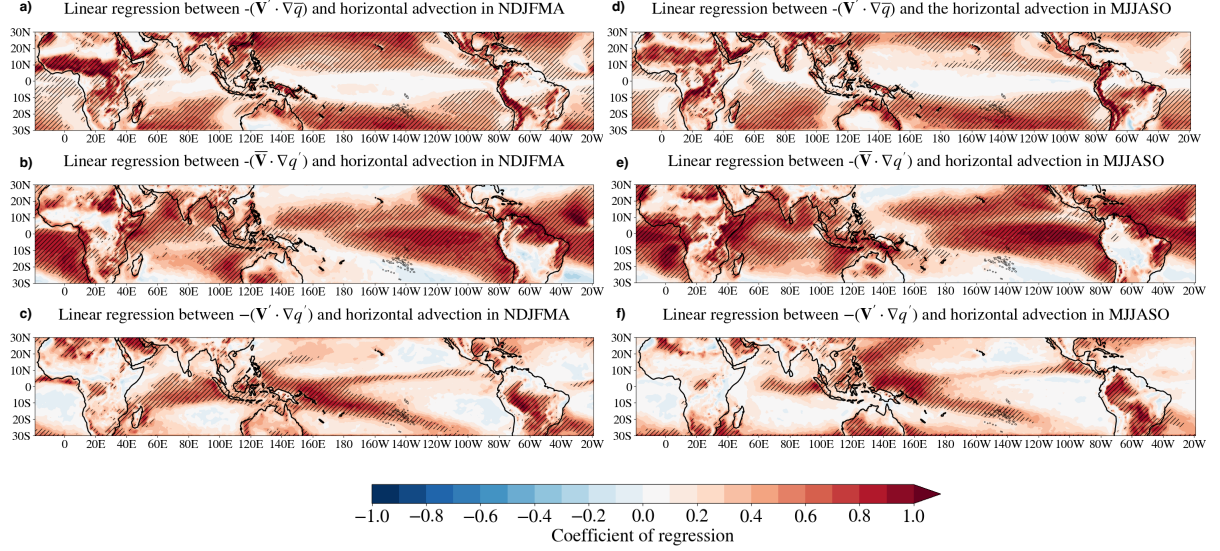

Fig. 7. Coefficient of regression (colour shading) and correlation (black stippling represents coefficient above 0.5) between horizontal advection anomalies at 950hPa and a) $\left(-\overrightarrow{V'}.\nabla\overline{q}\right)$ b) $\left(-\overrightarrow{\overline{V}}.\nabla q'\right)$ and c) $\left(-\overrightarrow{V'}.\nabla q'\right)$ and for NDJFMA. d)-e) for MJJASO.

The dominant contributor to horizontal advection across the subtropics is the anomalous wind acting on the climatological humidity field $\left(-\overrightarrow{V_{950}}'.\nabla\overline{q_{950}}\right)$ (Figure 7a,d). Elsewhere, especially in the tropical band, it is the climatological wind acting on anomalous specific humidity which contributes most to the horizontal advection $\left(-\overrightarrow{\overline{V_{950}}}.\nabla q_{950}'\right)$, (Figure 7b,e) with the $\left(-\overrightarrow{V_{950}}'.\nabla q_{950}'\right)$ non-linear term playing a more significant role in the convergence zones and over South America (Figure 7c,f).

To sum up, horizontal advection of the climatological moisture gradient by anomalous winds is a driver of MJO-related humidity changes, and by extension, of variations in Tw in the northern and southern tropics/subtropics. In regions above warm waters in the Indian and Pacific Oceans warm pool (where we observe a strong MJO convection signal), other terms in the moisture budget, such as evaporation and vertical advection, are likely to also play a role.

4. Summary and discussion

We have quantified the influence of the Madden-Julian Oscillation on intraseasonal variations of humid heat and heatwaves (based on the wet-bulb temperature, Tw) across the tropics and subtropics. Our analysis has revealed statistically significant (at the 95% confidence level) and robust anomalies of Tw (and other heat stress metrics, see SI, Suppl Fig. 16 and 17) associated with different MJO phases and seasons over most of the tropics and subtropics, indicating a widespread modulation of humid heat and humid heatwaves, and dry cold spells, by the MJO. Stronger absolute Tw anomalies are observed during boreal winter compared to summer, (Suppl Fig. 5) particularly over land masses in Africa and Asia, including higher latitudes in the Northern Hemisphere. However, the variability of normalised humid heat associated with the MJO is strongest in the tropics, particularly in the Indian and Pacific Oceans, for both extended boreal summer and winter. A striking result is that the MJO's influence extends far beyond regions directly affected by MJO-related precipitation and convection anomalies, influencing humid heat globally, likely through atmospheric equatorial Kelvin and Rossby waves. We expect the remote forcing of the MJO on (humid) heatwaves, and (dry) cold spells, to extend further poleward than the 30°N-30°S tropical/subtropical band analysed here, knowing the MJO's influence on mid-latitude weather regimes (Cassou, 2008; Lee & Grotjahn, 2019; Hsu et al., 2020; Marshall et al., 2022).

We found complex patterns of Tw anomalies during different MJO phases. During the boreal winter, in regions with strong convective signals, warm Tw anomalies tend to precede the peak in precipitation, following the patterns of the recharge and discharge of moisture associated with the eastward propagation of the MJO active zone. However, this relationship does not always hold during the boreal summer where the heart of the MJO is sometimes associated with negative Tw in regions where dry-bulb temperature exerts a stronger influence on humid heat than moisture. For both seasons, in regions with weak to no convective signals, the timing of the Tw anomalies differs, likely due to the differing dynamics of the MJO itself (Mayta & Adames Corraliza, 2023) and the different processes driving dry-bulb temperature and specific humidity variability. Furthermore, the intensity of Tw anomalies varies across regions and seasons. The seasonality of the anomalies is

primarily driven by changes in the background climate state across seasons, as well as the seasonal variation in the characteristics of the MJO itself (Adames et al., 2016). Forecasting intraseasonal humid heat several weeks in advance, a promising prospect based on our results, should thus be region and season specific. The relevance of our results might be expected to further increase with climate change, due to the overall increase of temperature and specific humidity in the tropics and subtropics and the increased MJO's predictability with global warming (Du et al., 2024).

We have shown that Tw anomalies are primarily driven by specific humidity, except in dry regions like deserts or regions with strong intra-seasonal dry-bulb variability. In the subtropics, a key driver of changes in specific humidity (and thus Tw) is the horizontal advection of the climatological moisture gradient by MJO-related anomalous winds, whereas in the equatorial region it is the climatological wind acting on anomalous specific humidity which contributes most to the horizontal advection. Over the warm waters in the tropical band where advection is not as significant, other processes such as evaporation and vertical advection are likely to play a contributing role as well.

Our results, by showing the broad and statistically significant impacts of the MJO on specific humidity, should also have implications for potential evapotranspiration (PET), and thus for land aridity, plants and vegetation at the intraseasonal timescale. This opens perspectives of forecast potential several weeks in advance to better inform and proactively advise managers and decision-makers of water resources, agriculture and crop, in addition to human health, wildlife and livestock managements.

Humid heat not only poses health and economic risks but is also a fundamental factor in human (and other animals) comfort and livability, as the quality of life of populations is strongly influenced by hot and humid environmental conditions. Tw, as an indicator of humid heat, is often used as a proxy for heat stress (Sherwood & Huber, 2010; Raymond et al., 2020; Buzan & Huber, 2020; Vecellio et al., 2022; Speizer et al., 2022; Vanos et al., 2023). Indeed, when using empirical heat stress indices such as the Heat Index (HI) or the simplified Wet Bulb Globe Temperature (sWBGT), we also observe significant anomalies across much of the globe for both heat stress indices (Suppl. Fig. 16 and 17). This shows that our approach with Tw not only effectively describes the intraseasonal variability of humid heat but also represents a valuable proxy for MJO-modulated heat stress. However, Tw assumes shaded, well-ventilated conditions and does not capture the full influence of wind or solar exposure.

Given the strong and widespread wind anomalies associated with the MJO (Suppl. Fig. 10), heat stress indices such as the Universal Thermal Climate Index (UTCI) which account for wind are likely to be more accurate and comprehensive. This highlights the importance of considering additional indices like UTCI in future studies aimed at disentangling the various contributors to heat stress.

Here we have focussed on quantifying daily mean intraseasonal anomalies, i.e. the overall 'day+night' humid heat felt by local populations. Looking at humid heatwaves as the prolonged ($\geq$3 days) extremes of those daily mean temperatures implies taking into account night time wet-bulb temperatures, which have been strongly linked to heat stress (Buzan & Huber, 2020; Di Napoli et al., 2019). We expect our results to be qualitatively valid also for the humid heat daily maximum (Ivanovich et al., 2022). The global-scale influence of MJO-modulated humid heat is reflected in the likelihood of humid heatwave days for the different MJO phases and seasons. This extremes' likelihood could thus be potentially forecasted weeks in advance, lead times that can potentially enable societal mitigation of such extremes.

Tw has nearly a one-to-one relationship with moist enthalpy (moist static energy at the surface) and its equivalent the surface equivalent potential temperature (θ_e), a crucial tropical meteorological variable known to favour atmospheric deep convection/precipitation and weather extremes (Raymond et al., 2021; Song et al., 2022). The influence of the MJO on humid heat and Tw has therefore also an impact on θ_e and thus possibly on certain mesoscale and synoptic-scale weather systems (e.g., tropical storms and cyclones). Further studies are needed on that as well as on a full moisture and heat budget near the surface.

In conclusion, this study has highlighted the important role of the MJO, as a primary source of intraseasonal climate variability, in shaping intraseasonal variations in humid heat and heatwaves across the global tropics and subtropics. Our findings have implications for understanding weather and climate variability and laying the groundwork for further studies on extreme humid heat events using finer temporal and spatial resolutions. To further develop and potentially improve forecast systems, it would be beneficial to delve deeper into the mechanisms driving humid heat dynamics across the different regions and seasons in future research.

The importance of further implementing and sustaining proper ocean/atmosphere observing/modelling/forecasting systems for the entire tropics and subtropics (Foltz et al., 2025), such as the Tropical Pacific Observing System (TPOS2020 Cravatte et al., (2015), cannot be understated. Developing artificial intelligence techniques (Bi et al., 2023; Lam et al., 2023), improved observing systems, numerical weather prediction models and ocean-atmosphere general circulation models (Bauer et al., 2015), could help to further improve intraseasonal forecasts of humid heat, notably based on the MJO. Such forecast improvements, combined with adaptation measures such as urban built environment resilience (Machard et al., 2020) and appropriate biomaterial engineering that consider not only temperature, but also specific humidity and its future increase with climate change, are crucial for mitigating the stronger-to-come impacts of climate change and weather extremes.

Data Availability Statement.

All datasets used in this study are open-source and available to be downloaded online. Information on how to access the ECMWF ERA5 dataset can be found here: https://www.ecmwf.int/en/forecasts/dataset/ecmwf-reanalysis-v5 , https://cloud.google.com/storage/docs/public-datasets/era5?hl=fr#data_access. The GPCP daily V1.3 (https://www.ncei.noaa.gov/products/global-precipitation-climatology-project, https://doi.org/10.5065/ZGJD-9B02) was downloaded from the Asia-Pacific Data Research Centre (APDRC) of the International Pacific Research Center (IPRC, Hawaii, US-Japan funded) at https://apdrc.soest.hawaii.edu/data/data.php. The OMI index dataset is provided by the NOAA PSL, Boulder, Colorado, USA, via their website: OMI Index : https://psl.noaa.gov/mjo/mjoindex/. The RMM index dataset is provided by the BOM and is available online: http://www.bom.gov.au/climate/mjo/graphics/rmm.74toRealtime.txt. The Python scripts used for the analyses are available on demand to the authors and are planned to be put open online.

REFERENCES

Adames, Á. F., Wallace, J. M., & Monteiro, J. M. (2016). *Seasonality of the Structure and Propagation Characteristics of the MJO*. https://doi.org/10.1175/JAS-D-15-0232.1

Barriopedro, D., García-Herrera, R., Ordóñez, C., Miralles, D. G., & Salcedo-Sanz, S. (2023). Heat Waves: Physical Understanding and Scientific Challenges. *Reviews of Geophysics*, *61*(2), e2022RG000780. https://doi.org/10.1029/2022RG000780

Bauer, P., Thorpe, A., & Brunet, G. (2015). The quiet revolution of numerical weather prediction. *Nature*, *525*(7567), 47–55. https://doi.org/10.1038/nature14956

Bi, K., Xie, L., Zhang, H., Chen, X., Gu, X., & Tian, Q. (2023). Accurate medium-range global weather forecasting with 3D neural networks. *Nature*, *619*(7970), 533–538. https://doi.org/10.1038/s41586-023-06185-3

Bretherton, C. S., Widmann, M., Dymnikov, V. P., Wallace, J. M., & Bladé, I. (1999). *The Effective Number of Spatial Degrees of Freedom of a Time-Varying Field*. https://journals.ametsoc.org/view/journals/clim/12/7/1520-0442_1999_012_1990_tenosd_2.0.co_2.xml

Brunner, L., & Voigt, A. (2024). Pitfalls in diagnosing temperature extremes. *Nature Communications*, *15*(1), 2087. https://doi.org/10.1038/s41467-024-46349-x

Buzan, J. R., & Huber, M. (2020). Moist Heat Stress on a Hotter Earth. *Annual Review of Earth and Planetary Sciences*, *48*(Volume 48, 2020), 623–655. https://doi.org/10.1146/annurev-earth-053018-060100

Buzan, J. R., Oleson, K., & Huber, M. (2015). Implementation and comparison of a suite of heat stress metrics within the Community Land Model version 4.5. *Geoscientific Model Development*, *8*(2), 151–170. https://doi.org/10.5194/gmd-8-151-2015

Camargo, S. J., Wheeler, M. C., & Sobel, A. H. (2009). *Diagnosis of the MJO Modulation of Tropical Cyclogenesis Using an Empirical Index*. https://doi.org/10.1175/2009JAS3101.1

Cassou, C. (2008). Intraseasonal interaction between the Madden–Julian Oscillation and the North Atlantic Oscillation. *Nature*, *455*(7212), 523–527. https://doi.org/10.1038/nature07286

Chen, X., Li, N., Liu, J., Zhang, Z., Liu, Y., & Huang, C. (2020). Changes in Global and Regional Characteristics of Heat Stress Waves in the 21st Century. *Earth's Future*, *8*(11), e2020EF001636. https://doi.org/10.1029/2020EF001636

Coffel, E. D., Horton, R. M., & Sherbinin, A. de. (2017). Temperature and humidity based projections of a rapid rise in global heat stress exposure during the 21st century. *Environmental Research Letters*, *13*(1), 014001. https://doi.org/10.1088/1748-9326/aaa00e

Cravatte, S., Ganachaud, A., Dewitte, B., & Hernandez, F. (2015). TPOS2020: Tropical Pacific observing system for 2020. *Editorial–May 2015–Special Issue Jointly Coordinated by Mercator Ocean and Coriolis Focusing on Ocean Observations*.

Davies-Jones, R. (2008). An Efficient and Accurate Method for Computing the Wet-Bulb Temperature along Pseudoadiabats. *Monthly Weather Review*, *136*(7), 2764–2785. https://doi.org/10.1175/2007MWR2224.1

Delaunay, A., & Christensen, H. (2022). Interpretable Deep Learning for Probabilistic MJO Prediction. *Geophysical Research Letters*, *49*. https://doi.org/10.1029/2022GL098566

Di Napoli, C., Pappenberger, F., & Cloke, H. L. (2019). *Verification of Heat Stress Thresholds for a Health-Based Heat-Wave Definition*. https://doi.org/10.1175/JAMC-D-18-0246.1

Du, D., Subramanian, A. C., Han, W., Chapman, W. E., Weiss, J. B., & Bradley, E. (2024). Increase in MJO predictability under global warming. *Nature Climate Change*, *14*(1), 68–74. https://doi.org/10.1038/s41558-023-01885-0

Dunne, J. P., Stouffer, R. J., & John, J. G. (2013). Reductions in labour capacity from heat stress under climate warming. *Nature Climate Change*, *3*(6), 563–566. https://doi.org/10.1038/nclimate1827

Dutheil, C., Lal, S., Lengaigne, M., Cravatte, S., Menkès, C., Receveur, A., Börgel, F., Gröger, M., Houlbreque, F., Le Gendre, R., Mangolte, I., Peltier, A., & Meier, H. E. M. (2024). The massive 2016 marine heatwave in the Southwest Pacific: An "El Niño–Madden-Julian Oscillation" compound event. *Science Advances*, *10*(41), eadp2948. https://doi.org/10.1126/sciadv.adp2948

Ebi, K. L., Capon, A., Berry, P., Broderick, C., Dear, R. de, Havenith, G., Honda, Y., Kovats, R. S., Ma, W., Malik, A., Morris, N. B., Nybo, L., Seneviratne, S. I., Vanos, J., & Jay, O. (2021). Hot weather and heat extremes: Health risks. *The Lancet*, *398*(10301), 698–708. https://doi.org/10.1016/S0140-6736(21)01208-3

Fan, X., Duan, Q., Shen, C., Wu, Y., & Xing, C. (2020). Global surface air temperatures in CMIP6: Historical performance and future changes. *Environmental Research Letters*, *15*(10), 104056. https://doi.org/10.1088/1748-9326/abb051

Foltz, G. R., Eddebbar, Y. A., Sprintall, J., Capotondi, A., Cravatte, S., Brandt, P., Sutton, A. J., Morris, T., Hermes, J., McMahon, C. R., McPhaden, M. J., Looney, L. B., Tuchen, F. P., Roxy, M. K., Wang, F., Chai, F., Rodrigues, R. R., Rodriguez-Fonseca, B., Subramanian, A. C., … Yu, W. (2025). Toward an integrated pantropical ocean observing system. *Frontiers in Marine Science*, *12*. https://doi.org/10.3389/fmars.2025.1539183

Gill, A. E. (1980). Some simple solutions for heat-induced tropical circulation. *Quarterly Journal of the Royal Meteorological Society*, *106*(449), 447–462. https://doi.org/10.1002/qj.49710644905

Gregory, C. H., Holbrook, N. J., Spillman, C. M., & Marshall, A. G. (2024). Combined Role of the MJO and ENSO in Shaping Extreme Warming Patterns and Coral Bleaching Risk in the Great Barrier Reef. *Geophysical Research Letters*, *51*(13), e2024GL108810. https://doi.org/10.1029/2024GL108810

Hafez, E. S. E. (1964). Behavioral thermoregulation in mammals and birds. *International Journal of Biometeorology*, *7*(3), 231–240. https://doi.org/10.1007/BF02187455

Hanna, E., & Tait, P. (2015). Limitations to Thermoregulation and Acclimatization Challenge Human Adaptation to Global Warming. *International Journal of Environmental Research and Public Health*, *12*(7), 8034–8074. https://doi.org/10.3390/ijerph120708034

Hersbach, H., Bell, B., Berrisford, P., Hirahara, S., Horányi, A., Muñoz-Sabater, J., Nicolas, J., Peubey, C., Radu, R., Schepers, D., Simmons, A., Soci, C., Abdalla, S., Abellan, X., Balsamo, G., Bechtold, P., Biavati, G., Bidlot, J., Bonavita, M., … Thépaut, J.-N. (2020). The ERA5 global reanalysis. *Quarterly Journal of the Royal Meteorological Society*, *146*(730), 1999–2049. https://doi.org/10.1002/qj.3803

Horton, D. E., Johnson, N. C., Singh, D., Swain, D. L., Rajaratnam, B., & Diffenbaugh, N. S. (2015). Contribution of changes in atmospheric circulation patterns to extreme temperature trends. *Nature*, *522*(7557), 465–469. https://doi.org/10.1038/nature14550

Hsu, P.-C., Qian, Y., Liu, Y., Murakami, H., & Gao, Y. (2020). Role of Abnormally Enhanced MJO over the Western Pacific in the Formation and Subseasonal Predictability of the Record-Breaking Northeast Asian Heatwave in the Summer of

2018. *Journal of Climate*, *33*(8), 3333–3349. https://doi.org/10.1175/JCLI-D-19-0337.1

Huffman, G. J., Adler, R. F., Morrissey, M. M., Bolvin, D. T., Curtis, S., Joyce, R., McGavock, B., & Susskind, J. (2001). Global Precipitation at One-Degree Daily Resolution from Multisatellite Observations. *Journal of Hydrometeorology*, *2*(1), 36–50. https://doi.org/10.1175/1525-7541(2001)002<0036:GPAODD>2.0.CO;2

IPCC. (2023). *IPCC, 2023: Climate Change 2023: Synthesis Report. Contribution of Working Groups I, II and III to the Sixth Assessment Report of the Intergovernmental Panel on Climate Change [Core Writing Team, H. Lee and J. Romero (eds.)]. IPCC, Geneva, Switzerland.* (First). Intergovernmental Panel on Climate Change (IPCC). https://doi.org/10.59327/IPCC/AR6-9789291691647

Ivanovich, C., Anderson, W., Horton, R., Raymond, C., & Sobel, A. (2022). The Influence of Intraseasonal Oscillations on Humid Heat in the Persian Gulf and South Asia. *Journal of Climate*, *35*(13), 4309–4329. https://doi.org/10.1175/JCLI-D-21-0488.1

Ji, F., Wu, Z., Huang, J., & Chassignet, E. P. (2014). Evolution of land surface air temperature trend. *Nature Climate Change*, *4*(6), 462–466. https://doi.org/10.1038/nclimate2223

Jiang, X., Adames, Á. F., Kim, D., Maloney, E. D., Lin, H., Kim, H., Zhang, C., DeMott, C. A., & Klingaman, N. P. (2020). Fifty Years of Research on the Madden-Julian Oscillation: Recent Progress, Challenges, and Perspectives. *Journal of Geophysical Research: Atmospheres*, *125*(17), e2019JD030911. https://doi.org/10.1029/2019JD030911

Kiladis, G. N., Dias, J., Straub, K. H., Wheeler, M. C., Tulich, S. N., Kikuchi, K., Weickmann, K. M., & Ventrice, M. J. (2014). A Comparison of OLR and Circulation-

Based Indices for Tracking the MJO. *Monthly Weather Review*, *142*(5), 1697–1715. https://doi.org/10.1175/MWR-D-13-00301.1

Kim, H., Vitart, F., & Waliser, D. E. (2018). *Prediction of the Madden–Julian Oscillation: A Review*. https://doi.org/10.1175/JCLI-D-18-0210.1

Kiranmayi, L., & Maloney, E. D. (2011). Intraseasonal moist static energy budget in reanalysis data. *Journal of Geophysical Research: Atmospheres*, *116*(D21). https://doi.org/10.1029/2011JD016031

Lam, R., Sanchez-Gonzalez, A., Willson, M., Wirnsberger, P., Fortunato, M., Alet, F., Ravuri, S., Ewalds, T., Eaton-Rosen, Z., Hu, W., Merose, A., Hoyer, S., Holland, G., Vinyals, O., Stott, J., Pritzel, A., Mohamed, S., & Battaglia, P. (2023). Learning skillful medium-range global weather forecasting. *Science*, *382*(6677), 1416–1421. https://doi.org/10.1126/science.adi2336

Lee, Y.-Y., & Grotjahn, R. (2019). Evidence of Specific MJO Phase Occurrence with Summertime California Central Valley Extreme Hot Weather. *Advances in Atmospheric Sciences*, *36*(6), 589–602. https://doi.org/10.1007/s00376-019-8167-1

Li, J., Chen, Y. D., Gan, T. Y., & Lau, N.-C. (2018). Elevated increases in human-perceived temperature under climate warming. *Nature Climate Change*, *8*(1), 43–47. https://doi.org/10.1038/s41558-017-0036-2

Lutsko, N. J. (2021). *The Relative Contributions of Temperature and Moisture to Heat Stress Changes under Warming*. https://doi.org/10.1175/JCLI-D-20-0262.1

Machard, A., Martinez, S., Bozonnet, E., Lacedra, E., & Inard, C. (2020). How to assess ecodistrict resilience to urban heat stress under future heatwaves? A case study for the city of Paris. *iCRBE Procedia*, 11–24. https://doi.org/10.32438/iCRBE.202044

Mapes, B. E., Chung, E. S., Hannah, W. M., Masunaga, H., Wimmers, A. J., & Velden, C. S. (2018). The Meandering Margin of the Meteorological Moist Tropics. *Geophysical Research Letters*, *45*(2), 1177–1184. https://doi.org/10.1002/2017GL076440

Marshall, A. G., Wheeler, M. C., & Cowan, T. (2022). Madden–Julian Oscillation Impacts on Australian Temperatures and Extremes. *Journal of Climate*, *36*(2), 335–357. https://doi.org/10.1175/JCLI-D-22-0413.1

Martin, Z. K., Barnes, E. A., & Maloney, E. (2022). Using Simple, Explainable Neural Networks to Predict the Madden-Julian Oscillation. *Journal of Advances in Modeling Earth Systems*, *14*(5), e2021MS002774. https://doi.org/10.1029/2021MS002774

Matsuno, T. (1966). Quasi-geostrophic motions in the equatorial area. *Journal of the Meteorological Society of Japan. Ser. II*, *44*(1), 25–43.

Matthews, T. K. R., Wilby, R. L., & Murphy, C. (2017). Communicating the deadly consequences of global warming for human heat stress. *Proceedings of the National Academy of Sciences of the United States of America*, *114*(15), 3861–3866. https://doi.org/10.1073/pnas.1617526114

Mayta, V. C., & Adames Corraliza, Á. F. (2023). Is the Madden-Julian Oscillation a Moisture Mode? *Geophysical Research Letters*, *50*(15), e2023GL103002. https://doi.org/10.1029/2023GL103002

Mora, C., Dousset, B., Caldwell, I. R., Powell, F. E., Geronimo, R. C., Bielecki, C. R., Counsell, C. W. W., Dietrich, B. S., Johnston, E. T., Louis, L. V., Lucas, M. P., McKenzie, M. M., Shea, A. G., Tseng, H., Giambelluca, T. W., Leon, L. R., Hawkins, E., & Trauernicht, C. (2017). Global risk of deadly heat. *Nature Climate Change*, *7*(7), 501–506. https://doi.org/10.1038/nclimate3322

NOAA, N. C. for E. I. (2025). *Monthly Global Climate Report for Annual 2024*. NOAA

National Centers for Environmental Information.

https://www.ncei.noaa.gov/access/metadata/landing-

page/bin/iso?id=gov.noaa.ncdc:C00672

Perkins, S. E., & Alexander, L. V. (2013). *On the Measurement of Heat Waves*.

https://doi.org/10.1175/JCLI-D-12-00383.1

Perkins, S. E., Alexander, L. V., & Nairn, J. R. (2012). Increasing frequency, intensity and

duration of observed global heatwaves and warm spells. *Geophysical Research*

Letters, *39*(20). https://doi.org/10.1029/2012GL053361

Perkins-Kirkpatrick, S. E., & Lewis, S. C. (2020). Increasing trends in regional heatwaves.

Nature Communications, *11*(1), 3357. https://doi.org/10.1038/s41467-020-16970-7

Peterson, T., Folland, C., Gruza, G., Hogg, W., Mokssit, A., & Plummer, N. (2001). *Report*

on the activities of the working group on climate change detection and related

rapporteurs. World Meteorological Organization Geneva.

Raymond, C., Matthews, T., & Horton, R. M. (2020). The emergence of heat and humidity

too severe for human tolerance. *Science Advances*, *6*(19), eaaw1838.

https://doi.org/10.1126/sciadv.aaw1838

Raymond, C., Matthews, T., Horton, R. M., Fischer, E. M., Fueglistaler, S., Ivanovich, C.,

Suarez-Gutierrez, L., & Zhang, Y. (2021). On the Controlling Factors for Globally

Extreme Humid Heat. *Geophysical Research Letters*, *48*(23), e2021GL096082.

https://doi.org/10.1029/2021GL096082

Raymond, C., Singh, D., & Horton, R. M. (2017). Spatiotemporal Patterns and Synoptics of

Extreme Wet-Bulb Temperature in the Contiguous United States. *Journal of*

Geophysical Research: Atmospheres, *122*(24), 13,108-13,124.
https://doi.org/10.1002/2017JD027140

Rogers, C. D. W., Ting, M., Li, C., Kornhuber, K., Coffel, E. D., Horton, R. M., Raymond, C., & Singh, D. (2021). Recent Increases in Exposure to Extreme Humid-Heat Events Disproportionately Affect Populated Regions. *Geophysical Research Letters*, *48*(19), e2021GL094183. https://doi.org/10.1029/2021GL094183

Russo, S., Sillmann, J., & Sterl, A. (2017). Humid heat waves at different warming levels. *Scientific Reports*, *7*(1), 7477. https://doi.org/10.1038/s41598-017-07536-7

Seneviratne, S. I., Donat, M. G., Mueller, B., & Alexander, L. V. (2014). No pause in the increase of hot temperature extremes. *Nature Climate Change*, *4*(3), 161–163. https://doi.org/10.1038/nclimate2145

Seo, K., & Kim, K. (2003). Propagation and initiation mechanisms of the Madden-Julian oscillation. *Journal of Geophysical Research: Atmospheres*, *108*(D13), 2002JD002876. https://doi.org/10.1029/2002JD002876

Sherwood, S. C. (2018). How Important Is Humidity in Heat Stress? *Journal of Geophysical Research: Atmospheres*, *123*(21). https://doi.org/10.1029/2018JD028969

Sherwood, S. C., & Huber, M. (2010). An adaptability limit to climate change due to heat stress. *Proceedings of the National Academy of Sciences*, *107*(21), 9552–9555. https://doi.org/10.1073/pnas.0913352107

Song, F., Zhang, G. J., Ramanathan, V., & Leung, L. R. (2022). Trends in surface equivalent potential temperature: A more comprehensive metric for global warming and weather extremes. *Proceedings of the National Academy of Sciences*, *119*(6), e2117832119. https://doi.org/10.1073/pnas.2117832119

Speizer, S., Raymond, C., Ivanovich, C., & Horton, R. M. (2022). Concentrated and

    Intensifying Humid Heat Extremes in the IPCC AR6 Regions. *Geophysical Research*

    Letters, *49*(5), e2021GL097261. https://doi.org/10.1029/2021GL097261

Vanos, J., Guzman-Echavarria, G., Baldwin, J. W., Bongers, C., Ebi, K. L., & Jay, O. (2023).

    A physiological approach for assessing human survivability and liveability to heat in a

    changing climate. *Nature Communications*, *14*(1), 7653.

    https://doi.org/10.1038/s41467-023-43121-5

Vecellio, D. J., Wolf, S. T., Cottle, R. M., & Kenney, W. L. (2022). Evaluating the 35°C wet-

    bulb temperature adaptability threshold for young, healthy subjects (PSU HEAT

    Project). *Journal of Applied Physiology*, *132*(2), 340–345.

    https://doi.org/10.1152/japplphysiol.00738.2021

Wang, L., Li, T., Chen, L., Behera, S. K., & Nasuno, T. (2018). Modulation of the MJO

    intensity over the equatorial western Pacific by two types of El Niño. *Climate*

    Dynamics, *51*(1–2), 687–700. https://doi.org/10.1007/s00382-017-3949-6

Wang, S., Ma, D., Sobel, A. H., & Tippett, M. K. (2018). Propagation Characteristics of

    BSISO Indices. *Geophysical Research Letters*, *45*(18), 9934–9943.

    https://doi.org/10.1029/2018GL078321

Wang, S., & Sobel, A. H. (2022). A Unified Moisture Mode Theory for the Madden–Julian

    Oscillation and the Boreal Summer Intraseasonal Oscillation. *Journal of Climate*,

    35(4), 1267–1291. https://doi.org/10.1175/JCLI-D-21-0361.1

Watanabe, M., & Jin, F.-F. (2003). *A Moist Linear Baroclinic Model: Coupled Dynamical–*

    Convective Response to El Niño.

    https://journals.ametsoc.org/view/journals/clim/16/8/1520-

    0442_2003_16_1121_amlbmc_2.0.co_2.xml

Wheeler, M. C., & Hendon, H. H. (2004). An All-Season Real-Time Multivariate MJO

    Index: Development of an Index for Monitoring and Prediction. *Monthly Weather*

    Review, *132*(8), 1917–1932. https://doi.org/10.1175/1520-

    0493(2004)132<1917:AARMMI>2.0.CO;2

White, C. J., Carlsen, H., Robertson, A. W., Klein, R. J. T., Lazo, J. K., Kumar, A., Vitart, F.,

    Coughlan de Perez, E., Ray, A. J., Murray, V., Bharwani, S., MacLeod, D., James, R.,

    Fleming, L., Morse, A. P., Eggen, B., Graham, R., Kjellström, E., Becker, E., …

    Zebiak, S. E. (2017). Potential applications of subseasonal-to-seasonal (S2S)

    predictions. *Meteorological Applications*, *24*(3), 315–325.

    https://doi.org/10.1002/met.1654

White, C. J., Domeisen, D. I. V., Acharya, N., Adefisan, E. A., Anderson, M. L., Aura, S.,

    Balogun, A. A., Bertram, D., Bluhm, S., Brayshaw, D. J., Browell, J., Büeler, D.,

    Charlton-Perez, A., Chourio, X., Christel, I., Coelho, C. A. S., DeFlorio, M. J.,

    Monache, L. D., Giuseppe, F. D., … Wilson, R. G. (2022). *Advances in the*

    Application and Utility of Subseasonal-to-Seasonal Predictions.

    https://doi.org/10.1175/BAMS-D-20-0224.1

Zhang, C. (2005). Madden-Julian Oscillation. *Reviews of Geophysics*, *43*(2).

    https://doi.org/10.1029/2004RG000158

Zhang, C. (2013). Madden–Julian Oscillation: Bridging Weather and Climate. *Bulletin of the*

    American Meteorological Society, *94*(12), 1849–1870.

    https://doi.org/10.1175/BAMS-D-12-00026.1

Zhang, C., Adames, Á. F., Khouider, B., Wang, B., & Yang, D. (2020). Four Theories of the

    Madden-Julian Oscillation. *Reviews of Geophysics*, *58*(3), e2019RG000685.

    https://doi.org/10.1029/2019RG000685

Zhang, Y., Boos, W. R., Held, I., Paciorek, C. J., & Fueglistaler, S. (2024). Forecasting Tropical Annual Maximum Wet-Bulb Temperatures Months in Advance From the Current State of ENSO. *Geophysical Research Letters*, *51*(7), e2023GL106990. https://doi.org/10.1029/2023GL106990

Zuo, J., Pullen, S., Palmer, J., Bennetts, H., Chileshe, N., & Ma, T. (2015). Impacts of heat waves and corresponding measures: A review. *Journal of Cleaner Production*, *92*, 1–12. https://doi.org/10.1016/j.jclepro.2014.12.078